A PASSIVE WIRELESS DIFFERENTIAL SENSOR FOR IN-SITU EARLY DETECTION OF PERIPROSTHETIC JOINT INFECTION

Jiaxin Jiang[1], Krithika Sureshkumar[1], Chandrashekhar Choudhary[1], Tristan Kerkes[1], H. Claude Sagi[2], Chia-Ying Lin[2], Michael T. Archdeacon[2], and Tao Li[1#]*

[1]Department of Electrical Engineering and Computer Science, University of Cincinnati, USA

[2]Department of Orthopaedic Surgery, University of Cincinnati, USA

ABSTRACT

This paper reports, for the first time, an implantable, passive wireless biosensor for *in situ* early detection of periprosthetic joint infection utilizing the magnetoelastic (ME) transduction mechanism combined with antibody-functionalization to target specific types of bacteria. A novel differential sensor configuration is introduced to distinguish the effects of target bacteria from variations caused by the surrounding medium. Differential operation of the sensor was successfully tested for mass detection in various media (air, water, standard 5cSt fluid, and paraffin oil), demonstrating effective elimination of medium effect by subtracting reference sensor outputs. A triangular geometry is adopted for the sensor design, replacing traditional rectangular shapes used in ME immunosensors to enhance the mass sensitivity and facilitate early infection detection. *In vitro* tests for proof of concept were carried out using single sensors in both rectangular and triangular shapes in *E. coli* suspension and PBS control solution, and successfully demonstrated a 2.63× improvement in mass sensitivity for the triangular sensors.

KEYWORDS

Magnetoelastic sensor, implantable device, resonant sensor, bacteria detection, mass loading, viscosity

INTRODUCTION

With an aging population, the increased number of total knee arthroplasty surgeries has been accompanied by a commensurate increase in revision surgeries – a large proportion of which are directly attributable to periprosthetic joint infection (PJI) [1]. The socioeconomic burden associated with PJI is not insignificant, with an estimated cost of up to $50k/patient and $250 million/year in the US [2]. To date, there is not one unanimously accepted approach for the diagnosis of PJI. Earlier studies have reported serum biomarkers and reduction in viscosity of microbial culture of synovial fluids as criteria to evaluate the infection progression [3-4]. However, the time required for these factors to reach levels sufficient for diagnosis is associated with further accumulation of pathogen and worsening infection. A wireless miniature biosensor that can enable real-time, *in vivo* detection of target bacteria, particularly during the early stages of infection (e.g. 48-72 hours after surgery), is thus highly desirable. Presently there is only limited research reported in this area. A hydrogel has been investigated for antigen sensitivity, intended to be integrated with an LC circuit for use as a wireless sensor for early detection of surgical site infection [5].

Magnetoelastic (ME) transduction has been employed in a broad range of sensing applications such as stress/strain measurements [6-7], pH sensing [8], cell growth monitoring [9], metal ion detection [10], and immunoassay for pathogens [11-12] and biomarkers [13]. With inherent passive wireless characteristics, ME sensors are highly suitable for implantable applications such as integration with orthopedic implants to monitor possible structural failures [14] and with biliary stents to monitor sludge accumulation and restenosis [15].

This paper reports an implantable, passive wireless biosensor for integration with a knee arthroplasty implant for *in situ* early detection of PJI. The sensor uses the ME transduction mechanism to enable passive wireless interrogation without the need for an antenna or local power source. Antibodies are immobilized on the sensor to target specific types of bacteria. Compared with existing ME immunosensors, a novel differential sensor configuration is used to distinguish the effects of target bacteria from variations caused by the surrounding medium. To enhance mass sensitivity and facilitate early infection detection, a triangular geometry is adopted for the sensor design, replacing traditional rectangular shapes used in ME immunosensors. *In vitro* tests for proof of concept have been performed for *Escherichia coli* (*E. coli)* detection and the measurement results are reported.

DEVICE DESIGN

The concept of the ME biosensor for *in situ* early detection of PJI is illustrated in Fig. 1. The wireless miniature ME biosensor is functionalized with antibodies targeting specific types of bacteria and mounted in a biocompatible package for integration into a recess on the prosthetic knee joint. The package, which has anchors to suspend the sensor inside, can prevent physical interference from tissue surrounding the implant area while allowing exchange of fluid through perforations on the package lid. The sensor is wirelessly interrogated using external coils that are interfaced with an external unit for sensor excitation and signal readout.

The working principle of the sensor for bacteria detection is shown in Fig. 2. A time-varying magnetic field from a transmit coil excites the ME sensor to produce a longitudinal vibration, which generates a magnetic flux with a resonance frequency that varies with changes in the mass and medium in contact with the sensor

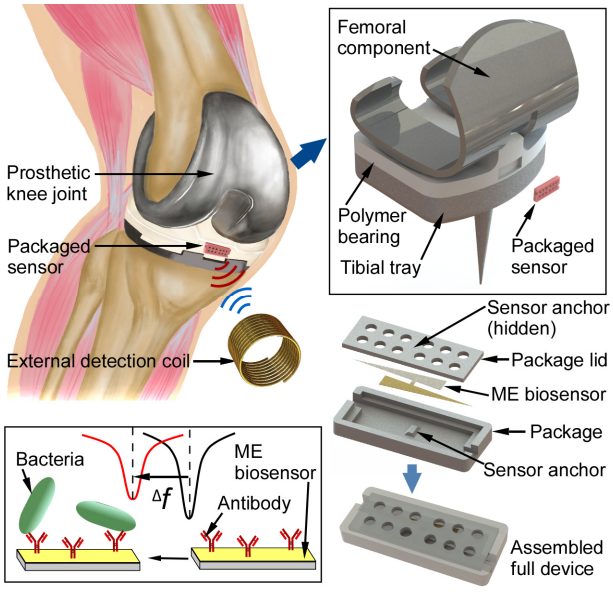

Figure 1: Device concept diagram of wireless biosensor for early PJI detection.

978-1-940470-04-7/HH2022/$25©2022TRF
DOI 10.31438/trf.hh2022.1

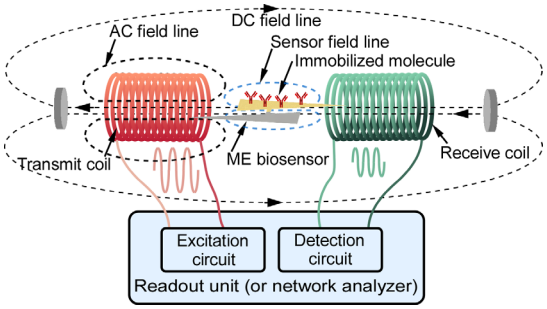

Figure 2: Schematic diagram showing detection and wireless readout methods of differential ME biosensor for bacteria detection. Network analyzer was used as readout unit for proof-of-concept experiments.

[16]. This flux can be detected wirelessly with a receive coil to measure the resonance frequency. Alternatively, a single coil can be used for both excitation and readout using signal reflection.

When a small amount of mass Δm is applied on the ME sensor of an initial mass M, the resonance frequency shift Δf can be derived from relationships given in [17] as

$$\Delta f = -\frac{\Delta m}{4LM}\sqrt{\frac{E}{\rho(1-\upsilon^2)}} \quad (1)$$

where L is the length of the sensor, E, ρ and υ are the Young's modulus, density and Poisson's ratio of the ME material, respectively.

ME sensors have been used as wireless high-performance immunosensors for *in vitro* applications, typically in an aqueous medium [11-13,18]. Changes in the medium properties and conditions such as temperature, density, viscosity, and pH, can cause significant changes in the resonance frequency of the ME immunosensors; therefore, these parameters are usually controlled carefully to maintain the sensor performance for immunoassay under *in vitro* conditions. However, for the targeted *in vivo* application, the properties of the surrounding body fluid, particularly the viscosity and density, can change at any time. To eliminate the effect of the surrounding medium, a novel differential sensor consisting of two ME sensors is utilized: one with, and the other without functionalized antibodies. The element without functionalization is used as a reference. When target bacteria are present in the medium and become bound to the antibodies, mass loading is applied only to the sensing element and any common mode changes such as those of the medium properties are eliminated by subtracting the outputs of the sensing and reference elements.

Mass sensitivity is defined as the frequency shift caused by a unit amount of mass loading. Higher mass sensitivity is desirable to provide a larger frequency shift for a given amount of mass loading, which is particularly important for the detection of bacteria during early stages of infection when the bacteria concentration is relatively low. It has been shown previously that the geometry of a ME sensor can affect its magnetic domain distribution; geometries with sharp corners can result in small magnetic domains, leading to stronger vibration and higher sensitivity [19]. As one of the methods investigated for mass sensitivity enhancement, triangular geometry is selected for the sensor design instead of the traditional rectangular geometry that has been commonly used for ME immunosensors.

The geometric design of the differential ME sensor is shown in Fig. 3, along with simulation results obtained using the COMSOL® Multiphysics software. A length difference of 0.6 mm between the sensing and reference elements is used to help separate the resonance frequency peaks of the two elements during signal readout. A spatial separation of 0.6 mm is also used to reduce the magnetic flux coupling between the two elements while keeping the

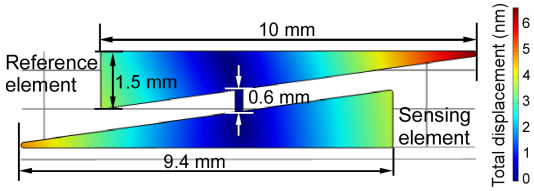

Figure 3: COMSOL® Multiphysics simulation of differential sensor configuration. Smaller displacement is observed for sensing element due to mass loading.

structure compact. A joint anchor that connects the two elements is placed at the 2/5 position from the base of each triangle where it is close to the null vibration point of the geometry. The simulation results shown in Fig. 3 along with others helped verify the differential sensor design as well as the improvement in mass sensitivity using the triangular geometry.

DEVICE FABRICATION

Ribbons of amorphous metallic glass (Metglas® 2826MB, $Fe_{45}Ni_{45}Mo_7B_3$ alloy from Metglas Inc.) were used as the ME material for sensor fabrication. The differential ME sensors were fabricated using an in-house high precision micro electro-discharge machine (Smaltec® EM203 µEDM). A 50 nm thick Cr layer followed by an 80 nm thick Au layer was then deposited on the sensing element of the differential sensors using e-beam evaporation with the reference element protected from deposition using photoresist. The Au surface provides a critical biocompatible layer for antibody immobilization while Cr serves as an adhesion layer with a larger-than-usual thickness to accommodate the surface roughness of the ME material.

Surface functionalization was performed by forming a self-assembled monolayer (SAM) on the Au surface using cysteamine (CYSTE) and then immobilizing antibodies on the SAM using crosslinking agents of N-(3-Dimethylaminopropyl)-N'-ethylcarbodiimide (EDC) and N-hydroxysulfosuccinimide (Sulfo-NHS) [20]. For this work, lyophilized cells of strain K12 *E. coli*, Sulfo-NHS, and bovine serum albumin (BSA) were purchased from Sigma Aldrich; CYSTE (98%), rabbit anti-*E. coli* polyclonal antibody, goat anti-rabbit antibody conjugated with Alexa Fluo® 488, and EDC were acquired from Fisher Scientific.

The functionalization procedure began with thorough cleaning

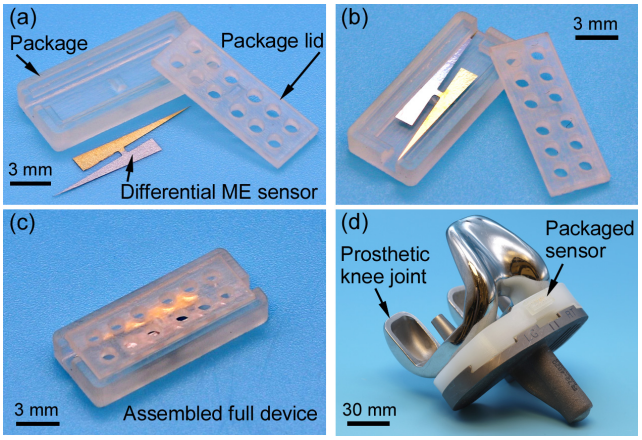

Figure 4: (a) Differential ME sensor (Metglas 2826MB) and package components (3D printed from VisiJet M3 resin); (b) sensor integrated on anchor inside package; (c) fully assembled device; (d) packaged device attached to prosthetic knee joint for demonstration of an intended integration site.

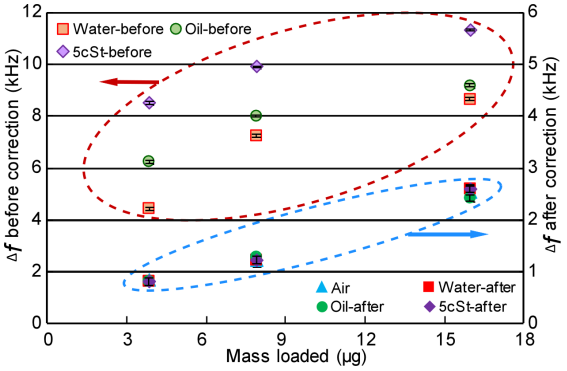

Figure 5: Measurement results showing characterization of differential ME biosensor for mass detection (ink coating) in different media and the effectiveness of eliminating medium effect on sensor response. The same mass loading generated different frequency shifts in various media before correction, which were effectively eliminated by subtracting reference element outputs. (Error bars too small to see. N=5)

of the ME sensors in an ultrasonic cleaner with a sequential use of acetone, IPA and DI water. The sensors were then immersed in a 20 mM CYSTE solution for 24 h to deposit the SAM. Anti-*E. coli* antibodies (2 μg/mL) were activated in a solution containing 0.01 mM EDC and 0.02 mM Sulfo-NHS for 2 h at 37°C. After washing with phosphate buffered saline (PBS, pH 7.4) to remove CYSTE molecules that did not adhere well, the ME sensors were soaked in the activated antibody solution to immobilize the antibodies on the sensors. Loosely bonded antibodies were removed by washing with PBS. To prevent non-specific binding during bacterial detection, the antibody-coated biosensors were further treated with a 1% w/w BSA solution for 30 min, rinsed with PBS to remove unbound BSA, and then dried under a nitrogen stream to make it ready for testing.

The package with perforated lid for the ME sensor was made by 3D printing from a biocompatible resin (VisiJet® M3). As shown in Fig. 4, two anchors in the package, one on the lid and the other on the inside bottom surface of the package, are used to clamp the differential sensor in the joint area, thus suspending it to prevent interference of the sensor vibration or blockage of the sensor functional surface. The packaged sensor can then be integrated in a recess formed on the prosthetic knee joint.

EXPERIMENTAL RESULTS

For all sensor experiments described below, two 40-turn coils of a 3/4 inch diameter made from 28 AWG magnet wire were used as the transmit and receive coils, respectively. A network analyzer (Keysight® E5061B) was connected to the two coils for sensor interrogation. The power of the excitation output from the network analyzer was 5 dBm and the received signal was processed by the network analyzer to generate the frequency response and thus the resonance frequency of the ME sensors.

Experiments were performed to verify the differential operation of the ME sensor and its capability to effectively eliminate the effect of varying medium properties. For these tests, mass loading was applied by coating multiple layers of ink on the sensing element of the differential sensors. The sensors were first tested in air to generate the baseline response and then tested in three different media (water, standard 5 cSt fluid, and paraffin oil) to emulate the impact of varying density and viscosity of the medium. The reference element outputs were scaled to correct for the frequency difference caused by the length mismatch in the sensor design, and then subtracted from the sensing element outputs to cancel the

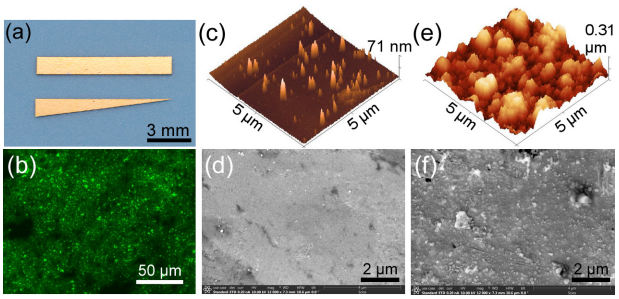

Figure 6: ME biosensor functionalization. (a) Photos of ME biosensors used for in vitro tests; (b) fluorescence microscopic image after antibody immobilization; (c) AFM and (d) SEM images of bare gold surface; (e) AFM and (f) SEM images after antibody immobilization.

medium effect. As demonstrated by the measurement results in Fig. 5, the same mass loading generated different frequency shifts in various media before correction (data points inside the red dashed circle). This can lead to serious discrepancy when interpreting the frequency response caused by mass loading. By subtracting the scaled outputs from the reference element in each medium, the medium effect was effectively eliminated (data points inside the blue dashed circle), demonstrating the validity of the differential sensor mechanism.

Imaging techniques including scanning electron microscope (SEM), atomic force microscope (AFM) and fluorescence microscope were used to verify the efficacy of surface functionalization on the ME sensor. As shown in Fig. 6 (c-d) and (e-f), the surface roughness of the sensor increased from 3.2 nm Ra on the bare gold surface to 62.7 nm after antibody immobilization. A secondary fluorescent antibody (goat anti-rabbit antibody conjugated with Alexa Fluo 488) was used to check the coverage of the primary antibody on the ME sensor using the Olympus IX81 microscope. The solution with the secondary antibody was diluted to a concentration of 4 μg/mL with PBS and then incubated with the functionalized ME biosensors. The fluorescent image in Fig. 6(b) verified the successful immobilization of the primary antibody on the sensor with satisfactory coverage.

In vitro tests were carried out for proof of concept for the detection of *E. coli* using single sensors. Both rectangular and right-angle triangular sensors with dimensions of 10 mm (L) × 1.5 mm (W) × 30 μm (T) were tested to demonstrate the improvement in sensitivity. Each ME sensor was first tested in 1 mL PBS solution for 30 minutes as control. Then 10 μL of *E. coli* suspension was added to the PBS solution and the resonance frequency was monitored for 50 min using a LabView program developed for data recording from the network analyzer. The concentration of the *E. coli* suspension was 8×10^6 cfu/mL determined by plate count. The test was repeated using 5 sensors and the results were averaged (N=5).

The *in vitro* test results for *E. coli* detection are plotted in Fig. 7. The control data was stable with a negligible frequency shift of <10 Hz. An average frequency shift of 97 Hz was obtained for the rectangular sensors during the testing period and 129 Hz for the triangular sensors. By estimating the number of *E. coli* cells attached to the sensor surfaces and assuming the mass of one *E. coli* cell to be 1 pg, the mass sensitivity can be calculated as 63 Hz/μg for the rectangular sensors and 166 Hz/μg for the triangular sensors. An improvement of 2.63× in mass sensitivity was observed for the triangular geometry compared to the traditional rectangular geometry.

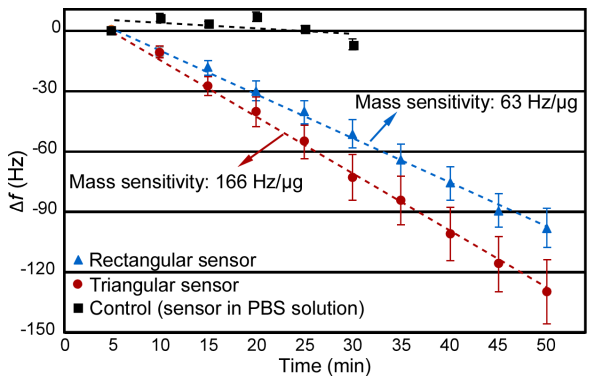

Figure 7: In-vitro test results for E. coli detection. Each sensor was tested in PBS solution for 30 min as control, then in E. coli suspension (8×10^6 cfu/ml determined by plate count) for 50 min. Data averaged from readings of 5 sensors (N=5). Error bar shows standard error. An improvement of 2.63× in mass sensitivity was observed for using the triangular geometry compared to the traditional rectangular geometry.

CONCLUSIONS

An implantable wireless biosensor for *in situ* early detection of PJI has been designed based on the ME transduction mechanism to enable passive wireless operation. The sensor can be functionalized to target specific types of bacteria that are known to be present during the early stages of PJI. A novel differential sensor configuration for distinguishing the effects of bacteria binding from variations caused by the surrounding medium was validated with experiments in emulated media. Triangular geometry was shown to enhance the mass sensitivity of the sensor over the traditional rectangular geometry. *In vitro* tests successfully demonstrated the capability of the sensor for detection of *E. coli* bacteria. Future works will focus on further improvement and characterization of sensor performance and integration, the capability to simultaneously target multiple types of bacteria, and evaluation of sensor characteristics for the *in vivo* environment.

ACKNOWLEDGEMENTS

This work was supported in part by internal funding at the University of Cincinnati. Facilities used for this work include the Mantei Research Center Cleanroom at the University of Cincinnati.

REFERENCES

[1] J. Gao, D. Xing, S. Dong, and J. Lin, "The primary total knee arthroplasty: A global analysis," *J. Orthopaedic Surgery and Research*, 15(190), 2020.

[2] C.R. Arciola, D. Campoccia, and L. Montanaro, "Implant infections: adhesion, biofilm formation and immune evasion," *Nature Rev. Microbiol.*, 16, 397-409, 2018.

[3] J. Fu, M. Ni, W. Chai, X. Li, L. Hao, and J. Chen, "Synovial Fluid Viscosity Test is Promising for the Diagnosis of Periprosthetic Joint Infection," *J. Anthroplasty*, 34(6), 1197-1200, 2019.

[4] J. Parvizi, T.L. Tan, K. Goswami, C. Higuera, C.D. Valle, A.F. Chen, and N. Shohat, "The 2018 Definition of Periprosthetic Hip and Knee Infection: An Evidence-Based and Validated Criteria," *J. Arthroplasty*, 33(5), 1309-1314.e2, 2018.

[5] E.A. Capogna, D.J. Munoz-Pinto, M.S. Hahn, and E.H. Ledet, "Identifying a crosslink density relationship of acrylamide hydrogels to be used with passive sensors for detecting periprosthetic infection," *41st Annual Northeast Biomedical Engineering Conference*, Troy, NY, USA, 2015.

[6] L. Liu, S. Zhang, Y. Qu, J. Zhou, F. Yang, R. Liu, and L. Liao, "Stress Monitoring of Prestressed Steel Strand Based on Magnetoelastic Effect Under Weak Magnetic Field Considering Material Strain," *Progress in Electromagnetics Research C*, 104, 157-170, 2020.

[7] L. Ren, K. Yu, and Y. Tan, "Wireless and Passive Magnetoelastic-Based Sensor for Force Monitoring of Artificial Bone," *IEEE Sensors Journal*, 19(6), 2096-2104, 2019.

[8] K.G. Ong, E.L. Tan, C.A. Grimes, and R. Shao, "Removal of Temperature and Earth's Field Effects of a Magnetoelastic pH Sensor," *IEEE Sensors Journal*, 8(4), 341-346, 2008.

[9] S. Shekhar, S.S. Karipott, R.E. Guldberg, and K.G. Ong, "Magnetoelastic sensors for real-time tracking of cell growth," *Biotechnology and Bioengineering*, 118(6), 2380-2385, 2021.

[10] X. Guo, S. Sang, A. Jian, S. Gao, Q. Duan, J. Ji, Q. Zhang, and W. Zhang, "A bovine serum albumin-coated magnetoelastic biosensor for the wireless detection of heavy metal ions," *Sensors and Actuators B: Chemical*, 256, 318-324, 2018.

[11] X. Huang, S. Sang, Z. Yuan, Q. Duan, X. Guo, H. Zhang, and C. Zhao, "A wireless biosensing microfluidic-chip based on resonating 'μ-diver'," *ACS Sens.*, 6(11), 3933-3939, 2021.

[12] L.V. Beltrami, M. Beltrami, M. Roesch-Ely, S.R. Kunst, F.P. Missell, E.J. Birriel, and C.D.F. Malfatti, "Magnetoelastic sensors with hybrid films for bacteria detection in milk," *J. Food Eng.,* 212, 18-28, 2017.

[13] R. Liu, X. Guo, J. Wang, J. Guo, Y. Zhang, W. Zhang, and S. Sang, "High sensitivity detection of human serum albumin using a novel magnetoelastic immunosensor," *Journal of Materials Science*, 54, 9679-9688, 2019.

[14] D.E. Mouzakis, D. Dimogianopoulos, and D. Giannikas, "Contact-Free Magnetoelastic Smart Microsensors with Stochastic Noise Filtering for Diagnosing Orthopedic Implant Failures," *IEEE Transactions on Industrial Electronics*, 56(4), 1092-1100, 2009.

[15] V. Pepakayala, J. Stein, and Y. Gianchandani, "Resonant magnetoelastic microstructures for wireless actuation of liquid flow on 3D surfaces and use in glaucoma drainage implants," *Microsystems & Nanoengineering*, 1, 15032, 2015.

[16] C.A. Grimes, S.C. Roy, S. Rani, and Q. Cai, "Theory, Instrumentation and Applications of Magnetoelastic Resonance Sensors: A review," *Sensors*, 11(3), 2809-2844, 2011.

[17] W. Shen, L. Mathison, V. Petrenko, and B. Chin, "Design and characterization of a magnetoelastic sensor for the detection of biological agents," *Journal of Physics D: Applied Physics*, 43(1), 015004, 2009.

[18] X. Huang, S. Sang, Z. Yuan, Q. Duan, X. Guo, H. Zhang, and C. Zhao, "Magnetoelastic Immunosensor via Antibody Immobilization for the Specific Detection of Lysozymes," *ACS Sens.*, 6(11), 3933-3939, 2021.

[19] P.G. Saiz, D. Gandia, A. Lasheras, A. Sagasti, I. Quintana, M. L. Fdez-Gubieda, J. Gutiérrez, M.I. Arriortua, and A.C. Lopes, "Enhanced mass sensitivity in novel magnetoelastic resonators geometries for advanced detection systems," *Sensors and Actuators: Chemical*, 296, 126612, 2019.

[20] M.D. Pozza, A.L. Possan, M. Roesch-Ely, and F.P. Missell, "Magneto-elastic biosensors: Influence of different thiols on pathogen capture efficiency," *Materials Science and Engineering C*, 75, 629-636, 2017.

CONTACT

*J. Jiang, tel: +1(513)208-3047; jiangj8@mail.uc.edu
#T. Li, tel: +1(513)556-3508; litao@uc.edu